

Avalanches, Clusters, and Structural Change in Cyclically Sheared Silica Glass

Himangsu Bhaumik^{1,*}, Giuseppe Foffi², and Srikanth Sastry^{1,†}¹Jawaharlal Nehru Center for Advanced Scientific Research, Jakkur Campus, Bengaluru 560064, India²Université Paris-Saclay, CNRS, Laboratoire de Physique des Solides, 91405 Orsay, France (Received 17 August 2021; revised 14 January 2022; accepted 9 February 2022; published 28 February 2022)

We investigate avalanches and clusters associated with plastic rearrangements and the nature of structural change in the prototypical strong glass, silica, computationally. We perform a detailed analysis of avalanches, and of spatially disconnected clusters that constitute them, for a wide range of system sizes. Although qualitative aspects of yielding in silica are similar to other glasses, the statistics of clusters exhibits significant differences, which we associate with differences in local structure. Across the yielding transition, anomalous structural change and densification, associated with a suppression of tetrahedral order, is observed to accompany strain localization.

DOI: 10.1103/PhysRevLett.128.098001

The mechanical response of amorphous solids such as metallic glasses, window glass, foams, emulsions, colloidal suspension, etc., to external deformation or applied stress is of central importance to characterize their behavior and determining their utility [1–3]. The response for large enough deformations involves plastic rearrangements, leading eventually to yielding. The yielding transition in amorphous solids has been investigated actively in recent years through experiments [4–8], numerical simulations [9–19] and theoretical investigations including analysis of elastoplastic and other models [20–31]. Yielding has been observed to be a discontinuous transition for sufficiently well annealed glasses under uniform shear [17] and for cyclic shear [15,18,32], accompanied by a discontinuous drop in energy and stress, and by localization of strain in shear bands [18,33–35].

Plasticity in amorphous solids is distinguished from that in crystalline solids [36] by the absence of well-defined structural defects with which it can be associated. Thus, the structural aspects of plastic rearrangements [18,37–41] have been a subject of investigation, to understand the structural motifs associated with plastic rearrangements below yielding, and to investigate the structural features that distinguish the regions in which plasticity is concentrated above the yielding transition.

Another aspect of the approach to yielding and steady state flow that has received considerable attention is the distribution of *avalanches* corresponding to plastic rearrangements [14,15,21,42,43], of interest also in a wide variety of phenomena exhibiting *crackling noise* [44]. The avalanche distribution is expected to have a power-law form, with a mean field prediction of exponent $\tau = 3/2$, and a characteristic cutoff that is finite below yielding. The scaling form has been rationalized by several elastoplastic models and mean-field theories constructed to pin down the scaling properties of avalanches [21,45–49]. In numerical

simulations, the avalanche distribution is found to be different across the yielding transition for cyclic shear [15], and to depend on factors such as the inertia of the system [50], shear rate [46], and the quantification of avalanche size (in terms of energy drops, or the size of the connected clusters of active particles) [15].

Plastic rearrangements in amorphous solids lead to long range stress fields [9,20,51,52], and thus long range interactions among regions of plastic activity. The implications of long range interactions on avalanches have been investigated in the context of depinning and crack propagation models [53,54], where it has been shown that such interactions lead nontrivially to avalanches being composed of spatially disconnected clusters. Similar investigations have not been performed for glasses, to our knowledge. We thus perform a detailed investigation of the statistics of avalanches, and of spatially disconnected clusters, for the archetypal glass, silica.

Relatively few studies [38,55–59] have addressed yielding behavior in silica, which is characterized by an open, tetrahedral, local geometry, and whose interaction potential includes long range Coulomb interactions (or silicon [60–63], which shares several geometric and thermodynamic characteristics), with most studies focusing on glasses composed of particles with spherically symmetric, short ranged interactions. In the liquid state, the tetrahedral network structure of silica entails a rich spectrum of novel behavior, including density maxima [64,65], a liquid-liquid phase transition [66,67] and a strong-to-fragile transition [68–71]. Studying silica is therefore of specific interest to understand the role of the nature of directional interactions and local tetrahedral geometry.

We find that the statistics of clusters is substantially different than those of avalanches, and confirm key observations made in [54]. In addition, we find such statistics for silica to be markedly different from that for

atomic glasses with short ranged interactions [15,72], despite broad similarities in their yielding behavior [32]. We attribute such differences to the local geometry in silica and discuss supporting evidence. It is therefore of interest to understand in detail the structure and structural change in silica across the yielding transition. We present results in this regard which highlight the unusual features of structural change in silica upon yielding.

We study a version of the Beest-Kramer-Santen (BKS) model introduced by Saika-Voivod [71,73] [see Supplemental Material (SM) for details [74]]. We prepared several equilibrated samples by performing constant volume, temperature (NVT) molecular dynamics simulations with an integration time step of 1 fs for a wide range of temperatures that straddles the threshold temperature $T_{th} = 3100$ K [32] for a fixed density $\rho = 2.8$ g/cm³. Avalanche properties display significant size dependence and, for this reason, we also simulate sizes ranging from $N = 1728$ to $N = 74088$. All the samples are equilibrated for at least $20\tau_\alpha$, τ_α being the structural relaxation time obtained from the self-intermediate scattering function $F_s(k, t)$. Inherent structures (energy minimum configurations) obtained from instantaneous quenches of equilibrated liquid configurations are then subjected to an athermal quasistatic shearing protocol involving two steps: (i) affine deformation by a small strain increments of $d\gamma = 2 \times 10^{-4}$ in the xz plane ($x' \rightarrow x + d\gamma z$, $y' \rightarrow y$, and $z' \rightarrow z$) and (ii) energy minimization. The procedure is then repeated and the strain γ is varied cyclically as $0 \rightarrow \gamma_{max} \rightarrow -\gamma_{max} \rightarrow 0$. Repeating the deformation cycle for a fixed strain amplitude γ_{max} , the glasses are driven to the steady state wherein properties of the system remain stable with further cycles of strain. We consider 12 samples for $N = 1728$, four samples for $N = 5832$ and 13 824, and one sample for $N = 27000$ and $N = 74088$ to perform the cyclic shear. We employ the conjugate-gradient algorithm for energy minimization and execute all the numerical simulations in LAMMPS [86].

We investigate avalanches by computing the statistics of *avalanche size* (S), *cluster size* (s), and the *number of clusters* (n_{cl}). The size of the avalanches is computed as the total number of *active* particles during a plastic rearrangement, identified by computing the deviatoric strain ϵ_d for each particle. Active particles are identified as those for which $\epsilon_d > 0.22$, following the procedure introduced in [87] [consistent results are obtained employing nonaffine displacements [15] for both silica and the Kob-Andersen binary Lennard-Jones glass (KA BMLJ), as shown in the SM]. We further obtain the sizes of clusters of connected active particles. Distributions of avalanche size and cluster size for $N = 1728$, several γ_{max} are shown in Fig. 1(a) and follow power laws with exponents close to $\tau_a = 1.1$ for avalanches and $\tau_c = 2$ for clusters, which do not change with γ_{max} , whereas the cutoffs do [2,44]. Strikingly, the cluster size exponent (τ_c) is significantly greater than the mean field avalanche exponent of $3/2$ [36], whereas τ_a is

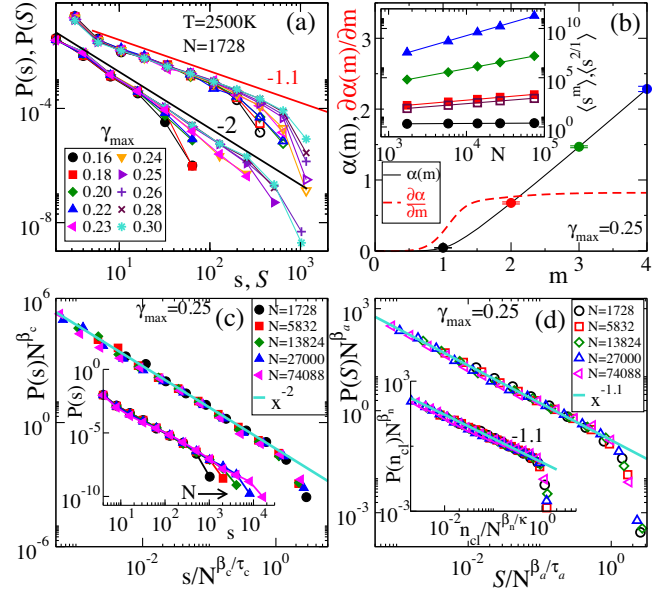


FIG. 1. (a) Distribution of avalanche size (open symbols) and clusters size (filled symbols) of active particles for $N = 1728$, $T = 2500$ K for several strain amplitudes γ_{max} (the yield amplitude $\gamma_{max}^Y = 0.23$). (b) Moment analysis of cluster size: the moment exponent (see text) $\alpha(m) = (\beta_c/\tau_c)(m + 1 - \tau_c)$ (black line) and $\partial\alpha(m)/\partial m$ (red dashed line) against m . Points are highlighted for integer values of m for which data of $\langle s^m \rangle$ against N are shown in the inset. The solid lines in the inset are the least squares fits to extract the value of $\alpha(m)$. Open squares represent the ratio of the second and first moments $\langle s^2 \rangle / \langle s \rangle$ which scales as $N^{0.63}$ and not $N^{1/3}$ as observed in other glasses [10,15,17]. (c) $P(s)N^{\beta_c}$ against $s/N^{\beta_c}/\tau_c$ for different system size N with $\tau_c = 1.9$ (see text) and $\beta_c/\tau_c = 0.79$. The solid line through the data points is a fit to $y \sim x^{-2}$. The inset shows the unscaled distributions for different system sizes. (d) Scaled avalanche size distribution $P(S)N^{\beta_a}$ for different system sizes with $\tau_a = 1.1$ and $\beta_a/\tau_a = 0.79$. Inset: Scaled distribution of the number of clusters for different system sizes with $\kappa = 1.12$ and $\beta_n/\kappa = 0.78$. Avalanches are collected in the first quadrant of the strain cycle.

significantly smaller. The distributions of energy drops, however, follow a power law with exponent ≈ -1.25 also observed for KA BMLJ [15] for which $\tau_c \approx 3/2$ (a summary of avalanche exponents found in different systems is included in the SM [74]).

In order to confirm these exponents, we perform a finite scaling analysis of the distributions of S , s , and n_{cl} , for $\gamma_{max} = 0.25$ (consistent results for other γ_{max} are shown in the SM). We assume a scaling form for cluster size

$$P(s) \approx N^{-\beta_c} f[s/N^{\beta_c}/\tau_c], \quad (1)$$

where the scaling function $f(x) \rightarrow x^{-\tau_c}$ for $x \rightarrow 0$, and $f(x) \rightarrow 0$ for $x \rightarrow 1$. This scaling form implies that the moments $\langle s^m \rangle \sim N^{\alpha(m)}$, where $\alpha(m) = \beta_c(m + 1 - \tau_c)/\tau_c$ is the moment exponent [88,89]. In the inset of Fig. 1(b),

we show a log-log plot of $\langle s^m \rangle$ against N for $m = 1, 2, 3$, and 4, from which we obtain $\alpha(m)$. In Fig. 1(b), we present $\alpha(m)$ and the corresponding derivative $\partial\alpha(m)/\partial m$ (which must equal β_c/τ_c for large m) as a function m , for $\gamma_{\max} = 0.25$ [$\alpha(m)$ values for $\gamma_{\max} = 0.28, 0.3$, shown in the SM, are nearly the same]. By a linear fit of $\alpha(m)$ in the large m range, we determine (averaging over $\gamma_{\max} = 0.25, 0.28$, and 0.3) $\beta_c/\tau_c = 0.79 \pm 0.02$ and $\beta_c = 1.70 \pm 0.10$, or $\tau_c = 2.15 \pm 0.07$. Figure 1(c) shows the excellent data collapse obtained by plotting scaled distributions $P(s, N)N^{\beta_c}$ against $s/N^{\beta_c/\tau_c}$, using $\tau_c = 1.9$ (rather than 2.15, for reasons explained below), for different system sizes N (equally good data collapse is obtained for choices $\tau_c = 2.15, 2$ as shown in the SM, Fig. S7). The collapsed data are best described by $\tau_c = 2$. We offer an analysis of the difference below, but note that the range 1.9 – 2.15 indicates the precision with which we can determine τ_c .

Assuming similar scaling forms for S and n_{cl} , we estimate $\tau_a = 1.1 \pm 0.05$, $\beta_a/\tau_a = 0.79 \pm 0.02$ for avalanche size, and $\kappa = 1.12 \pm 0.08$, $\beta_n/\kappa = 0.78 \pm 0.03$ for number of clusters [with $P(n_{\text{cl}}) \sim n_{\text{cl}}^{-\kappa}$]. In Fig. 1(d) we present the collapsed data for S and n_{cl} that confirm these exponents. We note that the observed equality $\beta_c/\tau_c = \beta_a/\tau_a$ is expected from the scaling functions considered, and is related to the fractal dimension as $d_f = d\beta/\tau$. The estimated values $d_f^{\text{est}} = 2.37$ for silica, and $d_f^{\text{est}} = 1.98$ for KA BMLJ (for which we find $\beta_a/\tau_a = 0.66$), are in close agreement with values obtained directly using the box counting method, $d_f = 2.22$, $d_f = 2$ for KA BMLJ (see SM Fig. S18).

We next discuss the relationship between these exponents. Considering $n(s|S)$, the number of clusters of size s in an avalanche of size S , we have, by definition, $\int_1^S s n(s|S) ds = S$ and $\int_1^S n(s|S) ds = n_{\text{cl}}(S)$. We assume (as supported by numerical data) that $n(s|S) \sim s^{-\tau_c}$ up to the cutoff S . We straightforwardly obtain $\langle n_{\text{cl}} \rangle_S \sim S^{\gamma_{ns}}$ with $\gamma_{ns} = \tau_c - 1$ and the mean cluster size $\langle s \rangle_S \sim S^{2-\tau_c}$. Data for several system sizes and S values, shown in Figs. 2(a) and 2(b), show that $\langle n_{\text{cl}} \rangle_S \sim S^{0.9}$ and $\langle s \rangle_S \sim S^{0.1}$, leading to $\tau_c = 1.9$, smaller than the value obtained by the moment

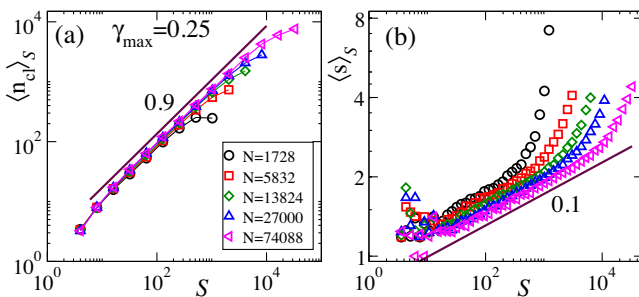


FIG. 2. (a) The average number of clusters $\langle n_{\text{cl}} \rangle_S$, and (b) the average cluster size $\langle s \rangle_S$, for given avalanche size S for different system sizes, follow $\langle n_{\text{cl}} \rangle_S \sim S^{\tau_c-1} \sim S^{0.9}$ and $\langle s \rangle_S \sim S^{2-\tau_c} \sim S^{0.1}$, leading to the estimate $\tau_c = 1.9$.

analysis. We consider this to be a more robust estimate, as it is based on integrals over $n(s|S)$, whose scaling depends only on τ_c . We attribute the difference with the *fit* value of $\tau_c = 2$ to the effect of the finite size cutoff function, whose form is generally not known. We obtain the form and demonstrate its effect on the fit exponent in the SM, Sec. S-5 C [74]. Further, assuming a scaling function $P(n_{\text{cl}}|S) \sim S^{-\gamma_{ns}} g(n_{\text{cl}}/S^{\gamma_{ns}})$ for the distribution of the number of clusters, we obtain

$$P(n_{\text{cl}}) = \int P(n_{\text{cl}}|S)P(S)dS \sim n_{\text{cl}}^{-\kappa}, \quad (2)$$

with $\kappa = 1 + (\tau_a - 1)/\gamma_{ns} = 1 + (\tau_a - 1)/(\tau_c - 1)$. The exponent values we obtain, $\gamma_{ns} = 0.9$, $\tau_c = 1.9$, $\tau_a = 1.1$, and $\kappa = 1.12$ clearly satisfy the exponent relationships we describe. Such consistency is also obtained for a two dimensional glass [72]. Despite such consistent analysis within the framework of [54], the large value of τ_c is surprising. Factors in addition to the long range elastic interactions may lead to a larger τ_c in silica, such as the long range interaction potential or the open, tetrahedral structure. Preliminary results for a short ranged silicalike model [90], shown in the SM, suggest the latter, which motivates a detailed investigation of structural change we present below. A more complete investigation of the resulting exponent values is involved, which we leave for future work.

We study the modification of structure under shear by considering the tetrahedrality parameter [91],

$$q_i = 1 - \frac{3}{8} \sum_{j>k} \left[\cos \theta_{jik} + \frac{1}{3} \right]^2, \quad (3)$$

that measures the tetrahedral order around a central Si atom i (with $q_i = 1$ for perfect tetrahedral order; see SM for details). We compute the distributions $P(q_i)$ for different γ_{\max} across the yielding transition, for $T = 2500$ and 6000 K, which are shown in Figs. 3(a) and 3(b). For $T = 2500$ K, the structure does not display any evolution for $\gamma_{\max} < \gamma_{\max}^Y$, with a peak at $q \sim 0.8$. Beyond yielding, the distributions evolve and become broader with increasing amplitude γ_{\max} , with a shoulder appearing around $q_i \simeq 0.4$ (reminiscent of the variation with temperature [91]). For $T = 6000$ K, Fig. 3(b), the behavior is very different. Below yielding, a strong enhancement of the tetrahedral order upon increasing γ_{\max} is observed, with the initial undeformed glass displaying very weak tetrahedral order. Beyond yield, as for $T = 2500$ K, the peak value decreases with γ_{\max} .

Next, we compute the mean and variance of q_i as a function of strain amplitude for different T as shown in Figs. 3(c) and 3(d), respectively. Below yielding, we observe two patterns. For $T > T_{\text{th}}$, $\langle q_i \rangle$ increases with γ_{\max} up to the yield amplitude. Interestingly, for all cases

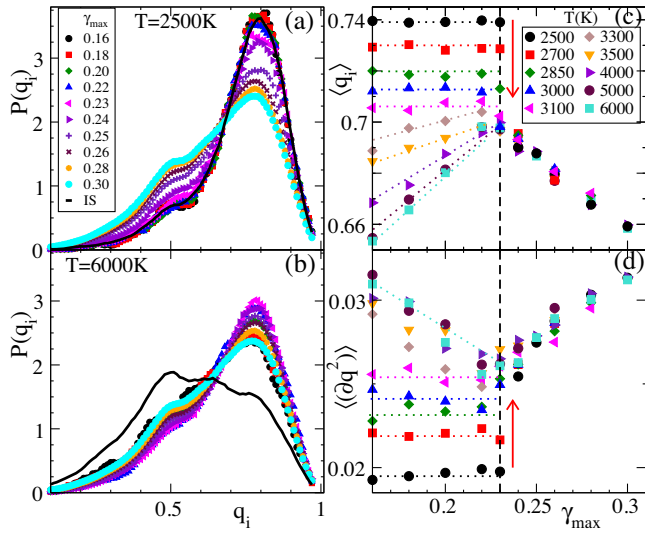


FIG. 3. Distributions $P(q_i)$ of the tetrahedrality parameter for zero strain configurations of cyclically deformed silica for different strain amplitude γ_{\max} for (a) $T = 2500\text{ K}$ and (b) $T = 6000\text{ K}$. (c) Averages $\langle q_i \rangle$ and (d) variances $\langle (\partial q)^2 \rangle = \langle q^2 \rangle - \langle q \rangle^2$, as a function of γ_{\max} for different temperatures T . Data are averaged over several configurations collected from different samples in the steady state for each γ_{\max} . The vertical dashed line indicates the yield strain, dotted lines through data points are a guide to the eyes and the arrows indicate the direction of increasing temperature.

with $T \geq T_{\text{th}}$, the maximum $\langle q_i \rangle = 0.7$ (attained at γ_{\max}^Y) equals the value of $\langle q_i \rangle$ for the undeformed samples at T_{th} (see Fig. S19 of SM). For $T < T_{\text{th}}$, $\langle q_i \rangle$ does not vary with γ_{\max} until the yield point where it abruptly drops to the same values as for the high temperature case. Above yielding, all the curves collapse, indicating that the final structure depends only on the strain amplitude, and $\langle q_i \rangle$ decreases with γ_{\max} . As shown in Fig. 3(c), the fluctuation of q_i also behaves in a similar way but in the opposite fashion, with a minimum at γ_{\max}^Y . These trends strikingly reflect the changes in the energy of the system [32]. The decrease of tetrahedral order in deformed silica can be explicitly linked to an increase in the population of five coordinated silicon atoms (see Sec. S-10 of SM, Fig. S20).

We next investigate structural features associated with strain localization [18] above γ_{\max}^Y . Figure 4(c) (inset) shows a snapshot of a zero strain configuration for $N = 74088$, $T = 2500\text{ K}$, and $\gamma_{\max} = 0.23$. The color map indicates the deviatoric strain ϵ_d , between consecutive stroboscopic configurations, up to a cutoff value 1.25 (see SM for a justification of this choice), highlighting the localization of strain in a shear band. We compute and plot the slabwise density $\langle \rho_x \rangle$ along the x direction in Fig. 4(a). Contrary to the observation in [18,41] for KA BMLJ, we find that $\langle \rho_x \rangle$ becomes progressively larger inside the shear band, with the number of cycles of shear. This reversal of trend reflects the fact that the energetically favorable tetrahedral structure of silica has lower density than more

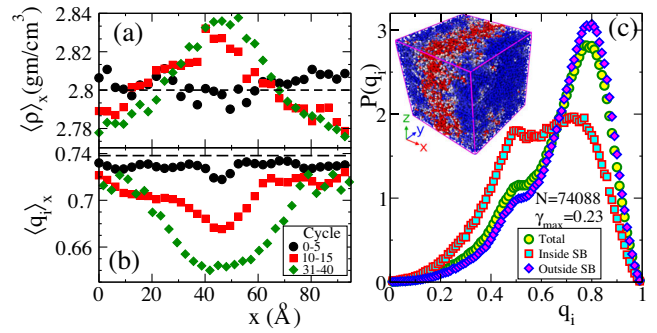


FIG. 4. (a) Slabwise averaged density $\langle \rho \rangle_x$ vs coordinate x . The dashed horizontal line at 2.8 g/cm^3 indicates the global density. (b) Slabwise averaged $\langle q_i \rangle_x$ vs x , averaged over consecutive cycles at three different windows. The dashed horizontal line indicates the value of q_i of the initial undeformed glass. (c) Distribution $P(q_i)$, for the total system, and for atoms inside and outside the shear band. To calculate the q_i inside the shear band, we consider those atoms whose $\epsilon_d > 1.25$. Inset: Snapshot of a steady state stroboscopic configuration for $\gamma_{\max} = 0.23$ for system size $N = 74088$ and $T = 2500\text{ K}$ (for which $\gamma_{\max}^Y \approx 0.2$). The color map indicates the deviatoric strain ϵ_d between successive stroboscopic configurations. Note that with periodic boundary conditions, the shear band can be oriented along the gradient, rather than the shear, direction.

disordered, higher energy structures, leading to density and other anomalies [91]. We compute slabwise averages of q_i , shown in Fig. 4(b), as well as the distributions of q_i within and outside the shear band [Fig. 4(c)], which confirm a lowering of orientational order within the shear band, analogous to observations in [40,92]. The reduced tetrahedral order within the shear band, analogous to high temperature undeformed glasses, is associated with the enhancement of the fraction of five coordinated defects (see Fig. S22 of SM).

In summary, we have investigated the statistics of avalanches and clusters in silica and obtained a satisfactory analysis of the relationship between exponents within a framework [54] that envisages the fragmentation of avalanches in the presence of long range interactions. We find that the cluster size exponent for silica is considerably larger than for atomic glasses investigated, which suggests that either the long range interactions in silica or the open tetrahedral geometry may additionally have an effect. A preliminary investigation of a short range silicalike model suggests that microscopic structure plays a role, but how microscopic structure (or other factors) may lead to the observed cluster statistics needs further investigation, including the study of other model systems. To elucidate further the anomalous structure and structural change in silica, we investigated structural change across the yielding transition and differences in structure within and outside shear bands. We find that yielding and the formation of shear bands is accompanied by a reduction of tetrahedral order, and corresponds to an anomalous increase

(rather than decrease) of density. Although the qualitative features of yielding—the role of annealing, formation of shear bands, etc.—in silica are analogous to other glasses [32], the peculiar features of local geometry in silica apparently lead to unusual cluster statistics and structural change during yielding. In turn, the cluster characteristics and morphology of avalanches may be expected to influence details of plasticity, yielding, and failure modes, inasmuch as avalanches form precursors to failure modes. Establishing such a connection is an important future direction.

We thank Jürgen Horbach, Stefano Zapperi, and especially Alberto Rosso for useful discussions and comments on the manuscript. We acknowledge Indo-French Center for the Promotion of Advanced Research (IFCPAR/CEFIPRA) Project 5704-1 for support, the Thematic Unit of Excellence on Computational Materials Science, and the National Supercomputing Mission facility (Param Yukti) at the Jawaharlal Nehru Center for Advanced Scientific Research for computational resources. S. S. acknowledges support through the J. C. Bose Fellowship (JBR/2020/000015) SERB, DST (India).

*Present address: Faculty of Mechanical Engineering, Technion, Haifa 32000, Israel.

†sastry@jncasr.ac.in

- [1] D. Bonn, M. M. Denn, L. Berthier, T. Divoux, and S. Manneville, *Rev. Mod. Phys.* **89**, 035005 (2017).
- [2] A. Nicolas, E. E. Ferrero, K. Martens, and J.-L. Barrat, *Rev. Mod. Phys.* **90**, 045006 (2018).
- [3] A. D. S. Parmar and S. Sastry, Mechanical behavior of glasses and amorphous materials, in *Advances in the Chemistry and Physics of Materials* (World Scientific Publishing Co Pte Ltd, Singapore, 2019), Chap. 21, pp. 503–527.
- [4] B. A. Sun, H. B. Yu, W. Jiao, H. Y. Bai, D. Q. Zhao, and W. H. Wang, *Phys. Rev. Lett.* **105**, 035501 (2010).
- [5] N. C. Keim and S. R. Nagel, *Phys. Rev. Lett.* **107**, 010603 (2011).
- [6] J. Antonaglia, W. J. Wright, X. Gu, R. R. Byer, T. C. Hufnagel, M. LeBlanc, J. T. Uhl, and K. A. Dahmen, *Phys. Rev. Lett.* **112**, 155501 (2014).
- [7] N. C. Keim, J. Hass, B. Kroger, and D. Wierker, *Phys. Rev. Research* **2**, 012004(R) (2020).
- [8] T. Bennin, E. Xing, J. Ricci, and M. D. Ediger, *Macromolecules* **53**, 8467 (2020).
- [9] C. E. Maloney and A. Lemaître, *Phys. Rev. E* **74**, 016118 (2006).
- [10] S. Karmakar, E. Lerner, and I. Procaccia, *Phys. Rev. E* **82**, 055103(R) (2010).
- [11] P. K. Jaiswal, I. Procaccia, C. Rainone, and M. Singh, *Phys. Rev. Lett.* **116**, 085501 (2016).
- [12] D. Fiocco, G. Foffi, and S. Sastry, *Phys. Rev. E* **88**, 020301(R) (2013).
- [13] N. V. Priezjev, *Phys. Rev. E* **87**, 052302 (2013).
- [14] I. Regev, J. Weber, C. Reichhardt, K. A. Dahmen, and T. Lookman, *Nat. Commun.* **6**, 8805 (2015).
- [15] P. Leishangthem, A. D. S. Parmar, and S. Sastry, *Nat. Commun.* **8**, 14653 (2017).
- [16] Y. Jin, P. Urbani, F. Zamponi, and H. Yoshino, *Sci. Adv.* **4** (2018).
- [17] M. Ozawa, L. Berthier, G. Biroli, A. Rosso, and G. Tarjus, *Proc. Natl. Acad. Sci. U.S.A.* **115**, 6656 (2018).
- [18] A. D. S. Parmar, S. Kumar, and S. Sastry, *Phys. Rev. X* **9**, 021018 (2019).
- [19] A. Barbot, M. Lerbinger, A. Lemaître, D. Vandembroucq, and S. Patinet, *Phys. Rev. E* **101**, 033001 (2020).
- [20] R. Dasgupta, H. G. E. Hentschel, and I. Procaccia, *Phys. Rev. Lett.* **109**, 255502 (2012).
- [21] J. Lin, E. Lerner, A. Rosso, and M. Wyart, *Proc. Natl. Acad. Sci. U.S.A.* **111**, 14382 (2014).
- [22] G. Parisi, I. Procaccia, C. Rainone, and M. Singh, *Proc. Natl. Acad. Sci. U.S.A.* **114**, 5577 (2017).
- [23] P. Urbani and F. Zamponi, *Phys. Rev. Lett.* **118**, 038001 (2017).
- [24] Z. Budrikis, D. F. Castellanos, S. Sandfeld, M. Zaiser, and S. Zapperi, *Nat. Commun.* **8**, 15928 (2017).
- [25] M. Popović, T. W. de Geus, and M. Wyart, *Phys. Rev. E* **98**, 040901(R) (2018).
- [26] H. J. Barlow, J. O. Cochran, and S. M. Fielding, *Phys. Rev. Lett.* **125**, 168003 (2020).
- [27] C. Liu, E. E. Ferrero, E. A. Jagla, K. Martens, A. Rosso, and L. Talon, *arXiv:2012.15310*.
- [28] S. Sastry, *Phys. Rev. Lett.* **126**, 255501 (2021).
- [29] K. Khirallah, B. Tyukodi, D. Vandembroucq, and C. E. Maloney, *Phys. Rev. Lett.* **126**, 218005 (2021).
- [30] M. Mungan and S. Sastry, *Phys. Rev. Lett.* **127**, 248002 (2021).
- [31] J. T. Parley, S. M. Fielding, and P. Sollich, *Phys. Fluids* **32**, 127104 (2020).
- [32] H. Bhaumik, G. Foffi, and S. Sastry, *Proc. Natl. Acad. Sci. U.S.A.* **118**, e2100227118 (2021).
- [33] Y. Shi and M. L. Falk, *Phys. Rev. Lett.* **95**, 095502 (2005).
- [34] K. Martens, L. Bocquet, and J.-L. Barrat, *Soft Matter* **8**, 4197 (2012).
- [35] R. Radhakrishnan and S. M. Fielding, *Phys. Rev. Lett.* **117**, 188001 (2016).
- [36] J. P. Sethna, M. K. Bierbaum, K. A. Dahmen, C. P. Goodrich, J. R. Greer, L. X. Hayden, J. P. Kent-Dobias, E. D. Lee, D. B. Liarte, X. Ni *et al.*, *Annu. Rev. Mater. Res.* **47**, 217 (2017).
- [37] D. Richard, M. Ozawa, S. Patinet, E. Stanifer, B. Shang, S. A. Ridout, B. Xu, G. Zhang, P. K. Morse, J.-L. Barrat, L. Berthier, M. L. Falk, P. Guan, A. J. Liu, K. Martens, S. Sastry, D. Vandembroucq, E. Lerner, and M. L. Manning, *Phys. Rev. Mater.* **4**, 113609 (2020).
- [38] S. Bonfanti, R. Guerra, C. Mondal, I. Procaccia, and S. Zapperi, *Phys. Rev. E* **100**, 060602(R) (2019).
- [39] D. V. Denisov, M. T. Dang, B. Struth, A. Zaccone, G. H. Wegdam, and P. Schall, *Sci. Rep.* **5**, 14359 (2015).
- [40] V. V. Vasisht, G. Roberts, and E. Del Gado, *Phys. Rev. E* **102**, 010604(R) (2020).
- [41] S. Mitra, A. D. S. Parmar, P. Leishangthem, S. Sastry, and G. Foffi, *J. Stat. Mech.* 2021, 033203 (2021).

- [42] K. A. Dahmen, Y. Ben-Zion, and J. T. Uhl, *Phys. Rev. Lett.* **102**, 175501 (2009).
- [43] N. Oyama, H. Mizuno, and A. Ikeda, *Phys. Rev. E* **104**, 015002 (2021).
- [44] J. P. Sethna, K. A. Dahmen, and C. R. Myers, *Nature (London)* **410**, 242 (2001).
- [45] E. A. Jagla, *Phys. Rev. E* **92**, 042135 (2015).
- [46] C. Liu, E. E. Ferrero, F. Puosi, J.-L. Barrat, and K. Martens, *Phys. Rev. Lett.* **116**, 065501 (2016).
- [47] E. Bouchbinder, J. S. Langer, and I. Procaccia, *Phys. Rev. E* **75**, 036108 (2007).
- [48] K. A. Dahmen, Y. Ben-Zion, and J. T. Uhl, *Nat. Phys.* **7**, 554 (2011).
- [49] S. Franz and S. Spigler, *Phys. Rev. E* **95**, 022139 (2017).
- [50] K. M. Salerno, C. E. Maloney, and M. O. Robbins, *Phys. Rev. Lett.* **109**, 105703 (2012).
- [51] J. D. Eshelby, *Proc. R. Soc. A* **241**, 376 (1957).
- [52] G. Picard, A. Ajdari, F. Lequeux, and L. Bocquet, *Eur. Phys. J. E* **15**, 371 (2004).
- [53] L. Laurson, S. Santucci, and S. Zapperi, *Phys. Rev. E* **81**, 046116 (2010).
- [54] C. Le Priol, P. Le Doussal, and A. Rosso, *Phys. Rev. Lett.* **126**, 025702 (2021).
- [55] F. Léonforte, A. Tanguy, J. P. Wittmer, and J.-L. Barrat, *Phys. Rev. Lett.* **97**, 055501 (2006).
- [56] B. Mantsi, A. Tanguy, G. Kermouche, and E. Barthel, *Eur. Phys. J. B* **85**, 304 (2012).
- [57] R. Renou, L. Soulard, E. Lescoute, C. Dereure, D. Loison, and J.-P. Guin, *J. Phys. Chem. C* **121**, 13324 (2017).
- [58] C. L. Rountree, D. Vandembroucq, M. Talamali, E. Bouchaud, and S. Roux, *Phys. Rev. Lett.* **102**, 195501 (2009).
- [59] S. Bonfanti, E. E. Ferrero, A. L. Sellarro, R. Guerra, and S. Zapperi, *Nano Lett.* **18**, 4100 (2018).
- [60] M. J. Demkowicz and A. S. Argon, *Phys. Rev. B* **72**, 245205 (2005).
- [61] M. J. Demkowicz and A. S. Argon, *Phys. Rev. B* **72**, 245206 (2005).
- [62] A. S. Argon and M. J. Demkowicz, *Philos. Mag.* **86**, 4153 (2006).
- [63] C. Fusco, T. Albaret, and A. Tanguy, *Phys. Rev. E* **82**, 066116 (2010).
- [64] C. Angell and H. Kanno, *Science* **193**, 1121 (1976).
- [65] H. E. Stanley, *Liquid Polymorphism* (John Wiley & Sons, New York, USA, 2013).
- [66] I. Saika-Voivod, F. Sciortino, and P. H. Poole, *Phys. Rev. E* **63**, 011202 (2000).
- [67] R. Chen, E. Lascaris, and J. C. Palmer, *J. Chem. Phys.* **146**, 234503 (2017).
- [68] J. Horbach and W. Kob, *Phys. Rev. B* **60**, 3169 (1999).
- [69] K.-U. Hess, D. Dingwell, and E. Rössler, *Chem. Geol.* **128**, 155 (1996).
- [70] A. Saksengwitt, J. Reinisch, and A. Heuer, *Phys. Rev. Lett.* **93**, 235701 (2004).
- [71] I. Saika-Voivod, F. Sciortino, and P. H. Poole, *Phys. Rev. E* **69**, 041503 (2004).
- [72] H. Bhaumik, G. Foffi, and S. Sastry, *J. Chem. Phys.* **156**, 064502 (2022).
- [73] B. W. H. van Beest, G. J. Kramer, and R. A. van Santen, *Phys. Rev. Lett.* **64**, 1955 (1990).
- [74] See Supplemental Material at <http://link.aps.org/supplemental/10.1103/PhysRevLett.128.098001> for details on the BKS silica model, characterization of the yielding transition, statistics of avalanches and clusters in silica and in the KA BMLJ, calculation of exponent relationships, fractal dimension, tetrahedrality order parameter, statistics of bond angles, and distorted structures associated with strain localization, which includes additional Refs. [75–85].
- [75] J. Lin, T. Gueudré, A. Rosso, and M. Wyart, *Phys. Rev. Lett.* **115**, 168001 (2015).
- [76] A. Lemaître and C. Caroli, *Phys. Rev. Lett.* **103**, 065501 (2009).
- [77] M. Talamali, V. Petäjä, D. Vandembroucq, and S. Roux, *Phys. Rev. E* **84**, 016115 (2011).
- [78] A. E. Lagogianni, C. Liu, K. Martens, and K. Samwer, *Eur. Phys. J. B* **91**, 104 (2018).
- [79] H. Xu, J. C. Andresen, and I. Regev, *Phys. Rev. E* **103**, 052604 (2021).
- [80] G. P. Shrivastav, P. Chaudhuri, and J. Horbach, *Phys. Rev. E* **94**, 042605 (2016).
- [81] T. Niiyama, M. Wakeda, T. Shimokawa, and S. Ogata, *Phys. Rev. E* **100**, 043002 (2019).
- [82] Z. Ge, R. Martone, L. Brandt, and M. Minale, *arXiv:2106.14341*.
- [83] T. B. Schröder, S. Sastry, J. C. Dyre, and S. C. Glotzer, *J. Chem. Phys.* **112**, 9834 (2000).
- [84] E. Lerner and I. Procaccia, *Phys. Rev. E* **79**, 066109 (2009).
- [85] M. J. Demkowicz and A. S. Argon, *Phys. Rev. Lett.* **93**, 025505 (2004).
- [86] S. Plimpton, *J. Comput. Phys.* **117**, 1 (1995).
- [87] K. M. Salerno and M. O. Robbins, *Phys. Rev. E* **88**, 062206 (2013).
- [88] M. De Menech, A. L. Stella, and C. Tebaldi, *Phys. Rev. E* **58**, R2677 (1998).
- [89] A. Chessa, H. E. Stanley, A. Vespignani, and S. Zapperi, *Phys. Rev. E* **59**, R12 (1999).
- [90] D. Coslovich and G. Pastore, *J. Phys. Condens. Matter* **21**, 285107 (2009).
- [91] M. S. Shell, P. G. Debenedetti, and A. Z. Panagiotopoulos, *Phys. Rev. E* **66**, 011202 (2002).
- [92] Y. Shi and M. L. Falk, *Phys. Rev. B* **73**, 214201 (2006).